An LCL Resonant Converter with PWM Control—Analysis, Simulation, and Implementation

G. S. N. Raju and Seshagirirao Doradla, *Senior Member, IEEE*

***Abstract*—A three element resonant converter capable of driving voltage type load with load independent operation is analyzed using state-space approach. Pulse width modulation is employed to control and regulate the output voltage. Closed-form solutions are obtained under steady state conditions. The experimental study of a prototype converter reveals complete agreement with the analytical and SPICE simulation results. Typical experimental oscillograms are given to verify the basic principles.**

I. Introduction

HIGH frequency dc-dc resonant converters are widely used in many space and radar power supplies owing to their small size and light weight. It has been shown in the literature that zero-voltage switching and the operation above resonant frequency (lagging power factor operation) gives minimum switching power losses [1], [2]. Recently there has been growing interest in the area of high frequency resonant converters using three or more resonant elements due to their distinct advantage of having load independent operation away from the resonant frequency [3]–[5].

Three element LCL resonant converter with capacitive output filter was proposed earlier [6]. Its simplified analysis was given in [7]. The operation of the converter with variable frequency control was reported in these papers. The purpose of this paper is to study the performance of the three element LCL resonant converter with capacitive output filter under pulse width modulation keeping the switching frequency constant, which is lacking in the literature.

II. Principle of Operation and Modes

Fig. 1 shows the basic circuit diagram of the full bridge LCL resonant converter with the capacitive output filter, and Fig. 2 shows the gating signals of FET's and the waveforms of variables marked in Fig. 1. All FET's are gated by a clock signal whose frequency determines the switching frequency f_s of the converter. FET's S_{12} and S_{22} are gated with a controllable delay τ, respectively, with reference to the gating of S_{11} and S_{21}. The time delay τ is the interval during which the voltage v_{AB} in Fig. 1 is either $+V_g$ or $-V_g$, and v_{AB} is zero during the remaining period. The output voltage is controlled by varying the delay τ.

Typical tank voltages and currents are shown in Fig. 2(b). To have a better understanding of the converter all devices are assumed to be ideal, and the turns ratio of the hf transformer is assumed to be 1. Therefore, the effect of switching devices can be represented by means of an equivalent truncated square wave voltage v_{AB} with the amplitude equal to $+V_g$ or $-V_g$ each occurring for an interval τ and zero for the remaining period. Further, since large capacitance C_o is used at the output, the output rectifier circuit can be represented by a square wave voltage source v_{Lp} of amplitude $+V_o$ or $-V_o$ depending on the direction of the current i_d. Thus, the converter can be represented by an equivalent circuit model as shown in Fig. 3.

TABLE I
Different Modes of Operation for the Equivalent Circuit of Fig. 3.

Mode	m	n	S_o	$\lvert i_d \rvert$
1	+1	+1	ON	> 0
2	0	+1	ON	> 0
3	-1	+1	ON	> 0
4	+1	-1	ON	> 0
5	0	-1	ON	> 0
6	-1	-1	ON	> 0
7	0	-	OFF	0
8	+1	-	OFF	0
9	-1	-	OFF	0

Under steady state conditions, the converter shows nine possible modes of circuit operation depending on the values of m and n of Fig. 3. Table I gives the conditions under which these modes are encountered. Under the proposed pulse width modulation control strategy, only four continuous conduction modes (ccm) and one discontinuous conduction mode (dcm) are encountered if lagging power factor operation is to be maintained. Fig. 4 shows the mode sequence diagram for the above operation in one cycle. These modes are also indicated in Fig. 2 along with the waveforms.

A. Mode 1: $t_0 \leq t < t_2$

This mode comprises of regenerative interval of duration $(t_1 - t_0)$ and power interval of duration $(t_2 - t_1)$. The resonant current i_{Ls} is sinusoidal with the time period $T_{os} = 2\pi\sqrt{L_s C_s}$ since v_{Lp} is clamped. During the power interval, the input source supplies energy to the resonant network and the load.

Manuscript received October 22, 1993; revised October 17, 1994.
G. S. N. Raju is with Radar "B," LRDE, Bangalore 560 093 India.
S. Doradla is with the Department of Electrical Engineering, Indian Institute of Technology, Kanpur 208 016 India.
IEEE Log Number 9408506.

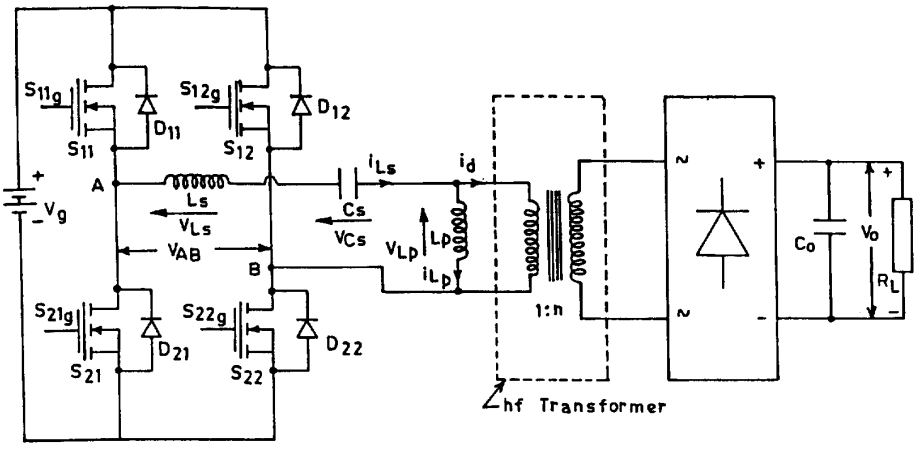

Fig. 1. Full bridge LCL converter.

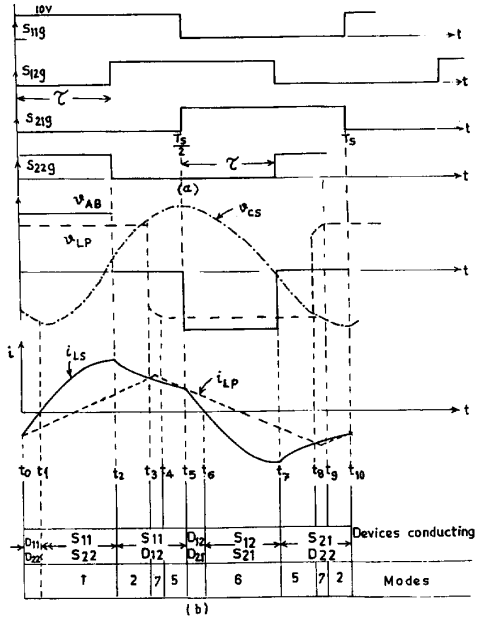

Fig. 2. Waveforms of different variables marked in Fig. 1. (a) Gating signals. (b) Waveforms of voltages and currents.

During the regenerative interval, the resonant network supplies energy back to the source while delivering the energy required by the load. The current through L_p increases linearly.

B. Mode 2: $t_2 \leq t < t_3$

This forms part of the free resonant interval during which the input voltage v_{AB} is shorted by switches S_{11} and D_{12}, and the resonant current i_{Ls} freewheels.

C. Mode 7: $t_3 \leq t < t_4$

This is a discontinuous mode which occurs at light loads for this scheme under pulse width control. Depending on the capacitor voltage at $t = t_3$, the output diode bridge does not conduct till $v_{Lp}(= |v_{Cs}|(L_p/(L_p + L_s)))$ is equal to V_o. During this mode the resonant network oscillates with the time period $T_o = 2\pi\sqrt{(L_s + L_p)C_s}$.

Modes 6 and 5 are similar to modes 1 and 2, respectively, for the second half cycle of converter operation.

III. Analysis

A. Nomenclature

E_{ri}	Input energy
E_{r0}	Output energy
K_L	Inductance ratio (L_p/L_s)
Q_E	Effective quality factor
M_o	Normalized output voltage (V_o/V_g)
M_{Cn}	Normalized capacitor voltage at $t = t_n$, $n = 0, 1, \cdots$
f_{no}	Optimum normalized switching frequency, $\sqrt{(1 + K_L)}$
f_o	$1/[2\pi\sqrt{((L_s + L_p)C_s)}]$
f_{os}	$1/[2\pi\sqrt{L_sC_s}]$
Z_o	$\sqrt{((L_s + L_p)/C_s)}$
Z_{os}	$\sqrt{(L_s/C_s)}$

B. State-Space Analysis

The equivalent circuit shown in Fig. 3 is used for the analysis. The vector space equation for the converter is

$$\dot{X} = AX + BU \tag{1}$$

where

$$A = \begin{bmatrix} 0 & -1/L_s & 0 \\ 1/C_s & 0 & 0 \\ 0 & 0 & 0 \end{bmatrix}$$

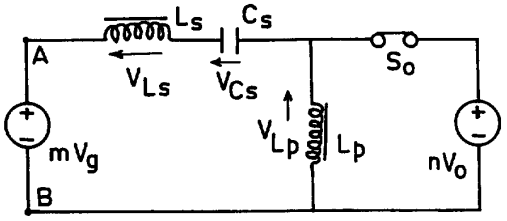

Fig. 3. Equivalent circuit model of LCL converter.

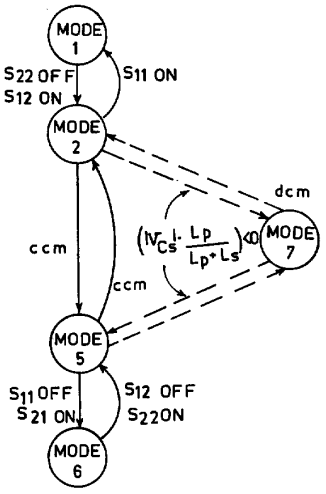

Fig. 4. Mode sequence diagram.

$$X = \begin{bmatrix} i_{Ls} \\ v_{Cs} \\ i_{Lp} \end{bmatrix}$$

$$B = \begin{bmatrix} m/L_s & -n/L_s \\ 0 & 0 \\ 0 & n/L_p \end{bmatrix}$$

$$U = \begin{bmatrix} V_g \\ V_o \end{bmatrix}$$

where m and n take values as shown in Table I representing different modes of continuous and discontinuous conduction.

However, in the discontinuous conduction mode 7, the converter operates like a simple series resonant converter with resonant frequency f_o and $i_{Ls} = i_{Lp}$. It is interesting to note that in all six continuous conduction modes, the voltage v_{Lp} is clamped and the current i_{Lp} is independent of the other two state variables. As a result, the third order matrix (1) can be reduced to second order equation for which the solutions are readily available [2].

The general solutions of (1) in the time interval $t_{p-1} \leq t < t_p$ are

$$i_{Ls}(t) = i_{Ls}(t_{p-1})\cos[\omega_{os}(t - t_{p-1})] + ((mV_g - nV_o - v_{Cs}(t_{p-1}))/Z_{os})\sin[\omega_{os}(t - t_{p-1})] \quad (2)$$

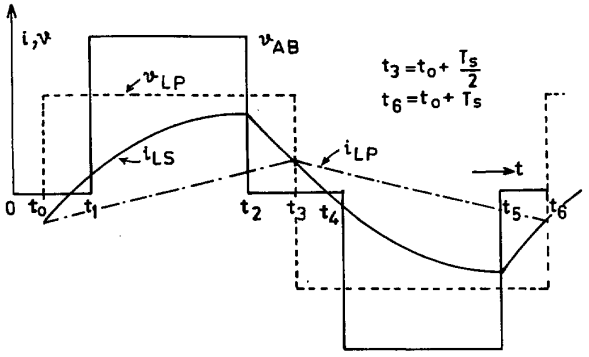

Fig. 5. Theoretical waveforms.

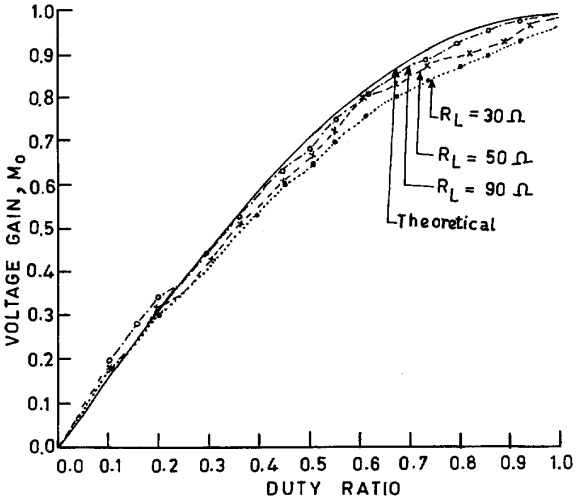

Fig. 6. Variation of voltage gain with the duty ratio.

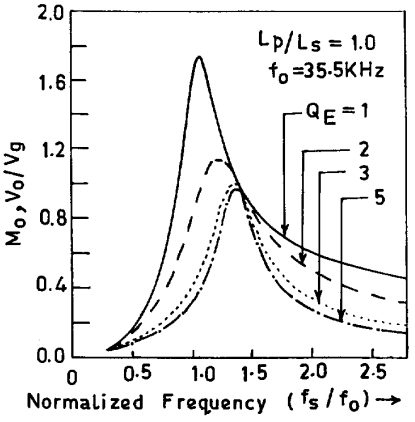

Fig. 7. Transfer characteristic of LCL converter.

$$v_{Cs}(t) = i_{Ls}(t_{p-1})Z_{os}\sin[\omega_{os}(t - t_{p-1})] + (mV_g - nV_o)[1 - \cos[\omega_{os}(t - t_{p-1})]] + v_{Cs}(t_{p-1})\cos[\omega_{os}(t - t_{p-1})] \quad (3)$$

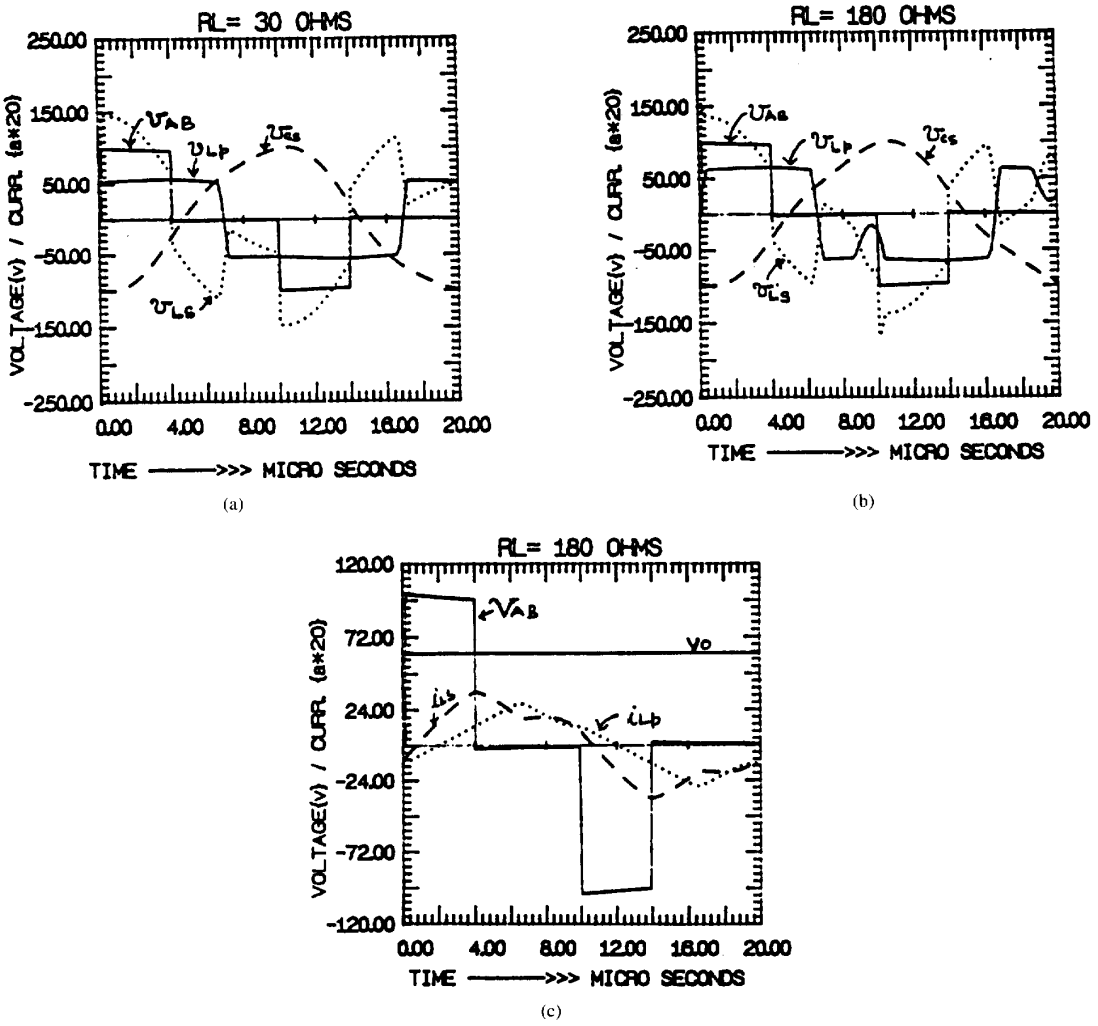

Fig. 8. Simulation waveforms for duty ratio of 0.4. (a) $R_L = 30\ \Omega v_{AB}, v_{Ls}, v_{cs}, v_{Lp}$. (b) $R_L = 180\ \Omega\ v_{AB}, v_{Ls}, v_{cs}, v_{Lp}$. (c) $R_L = 180\ \Omega v_{AB}, i_{Ls}, i_{Lp}, V_o$.

$$i_{Lp}(t) = i_{Lp}(t_{p-1}) + (n/L_p)V_o(t - t_{p-1}) \tag{4}$$

where

t_{p-1} is the time at the start of any ccm.
t_p is the time at the end of the same ccm.

Similarly, the solutions for the discontinuous conduction mode are

$$i_{Ls}(t) = i_{Lp}(t) = i_{Ls}(t_{p-1})\cos[\omega_o(t - t_{p-1})] + ((mV_g - v_{Cs}(t_{p-1}))/Z_o)\sin[\omega_o(t - t_{p-1})] \tag{5}$$

$$V_{Cs}(t) = i_{Ls}(t_{p-1})Z_o \sin[\omega_o(t - t_{p-1})] + mV_g[1 - \cos[\omega_o(t - t_{p-1})]] + v_{Cs}(t_{p-1})\cos[\omega_o(t - t_{p-1})]. \tag{6}$$

Fig. 5 shows the theoretical waveforms of the converter under continuous conduction mode (ccm).

C. Closed Form Equation for M_o

It can be seen from Fig. 1 and waveforms of Fig. 5, the load current is equal to average rectified i_d assuming ideal hf transformer with turns ratio $n = 1$. Therefore,

$$V_o/R_L = (2/T_s)\int_{t_o}^{t_o+T_s/2} i_d(t)\,dt \tag{7}$$

where

$$i_d = i_{Ls} - i_{Lp}. \tag{8}$$

The time t_o is conveniently selected at the instant where v_{Lp} changes from negative to positive. Therefore, the average current through L_p over one half cycle is zero. Also, the integral of $i_{Ls}(t)$ over half cycle is equal to charge flowing through the capacitance C_s from $t = t_o$ to $t = t_o + T_s/2$. With

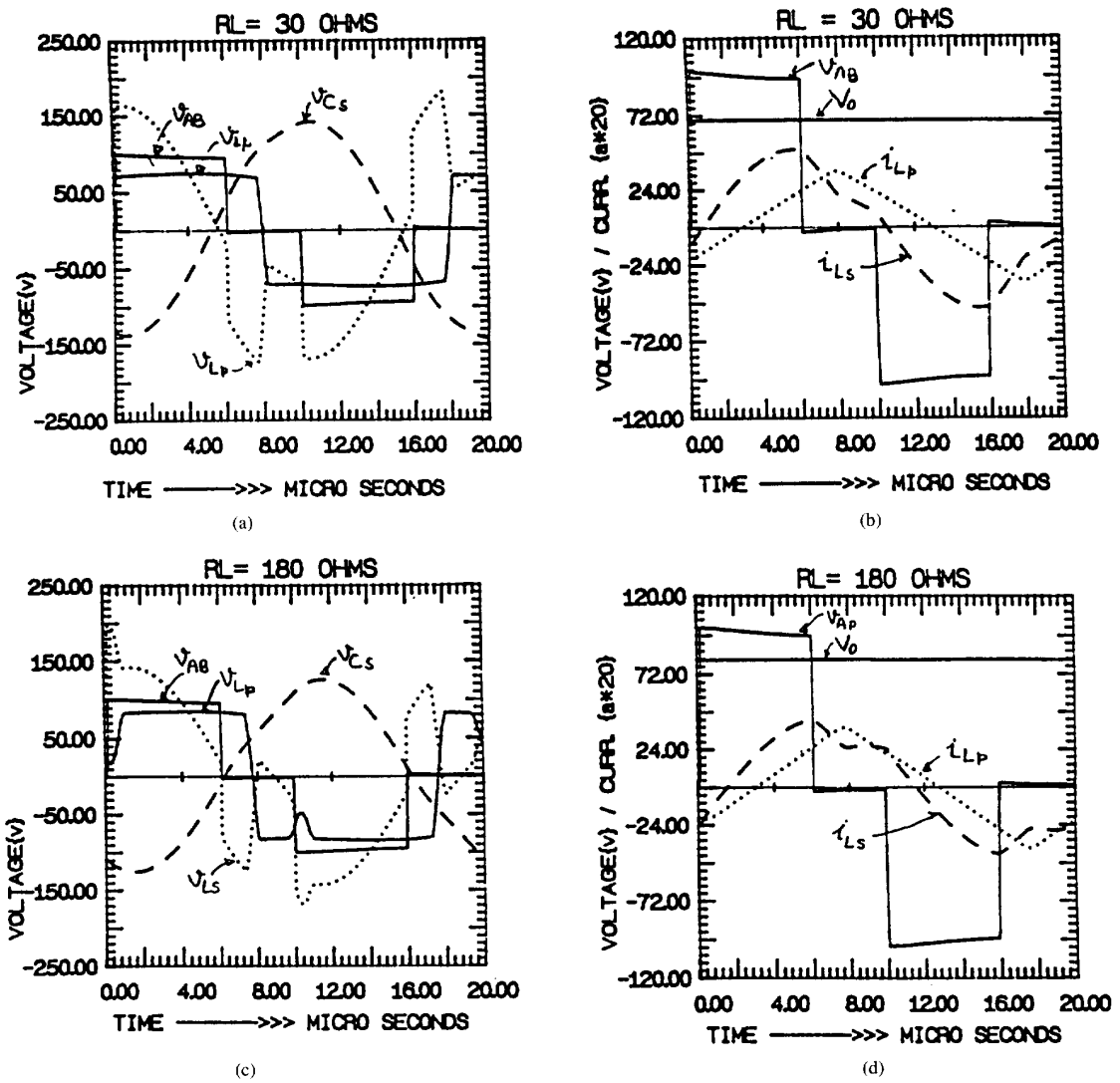

Fig. 9. Simulation waveforms for duty ratio of 0.6. (a) $R_L = 30\ \Omega v_{AB}, v_{Ls}, v_{cs}, v_{Lp}$. (b) $R_L = 30\ \Omega\ v_{AB}, i_{Ls}, i_{Lp}, V_o$. (c) $R_L = 180\ \Omega\ v_{AB}, v_{Ls}, v_{cs}, v_{Lp}$. (d) $R_L = 180\ \Omega\ v_{AB}, i_{Ls}, i_{Lp}, V_o$.

these observations (7) can be written as

$$V_o/R_L = 2(C_s/T_s)[v_{Cs}((T_s/2) + t_o) - v_{Cs}(t_o)]. \quad (9)$$

Normalizing (9) after substituting $v_{Cs}((T_s/2) + t_o) = -v_{Cs}(t_o)$

$$(M_o/M_{Co}) = -(2R_{Ln}f_{no})/\pi. \quad (10)$$

The input energy is

$$E_{Ri} = V_g \int_{t_o}^{t_o+T_s/2} i_{Ls}(t)\,dt = V_g C_s[V_{Cs}(t_2) - V_{Cs}(t_1)]. \quad (11)$$

The output energy is

$$E_{Ro} = V_o \int_{t_o}^{t_o+T_s/2} [i_{Ls}(t) - i_{Lp}(t)]\,dt = V_o C_s(-2V_{Cs}(t_o)). \quad (12)$$

Equating input energy (11) and output energy (12) and normalizing

$$M_{C2} - M_{C1} = -2M_oM_{Co} \quad (13)$$

where M_{C2} and M_{C1} denote normalized capacitor voltage at the instants t_2 and t_1, respectively. Using (10) and (13) and solutions of operating modes 2 to 6, the capacitor voltage at instants t_1 and t_2 is calculated in terms of M_{Co} and M_o. The final expressions are

$$M_{C2} - M_{C1} = -2M_oM_{Co} = M_o^2(\pi/R_{Ln}f_{no})) \quad (14)$$

$$M_o = sin\,((\pi/2)D) \quad (15)$$

where D is the duty cycle $= \tau/(T_s/2)$

From (15), it can be concluded that the output voltage is not dependent on the load resistance and the converter gain

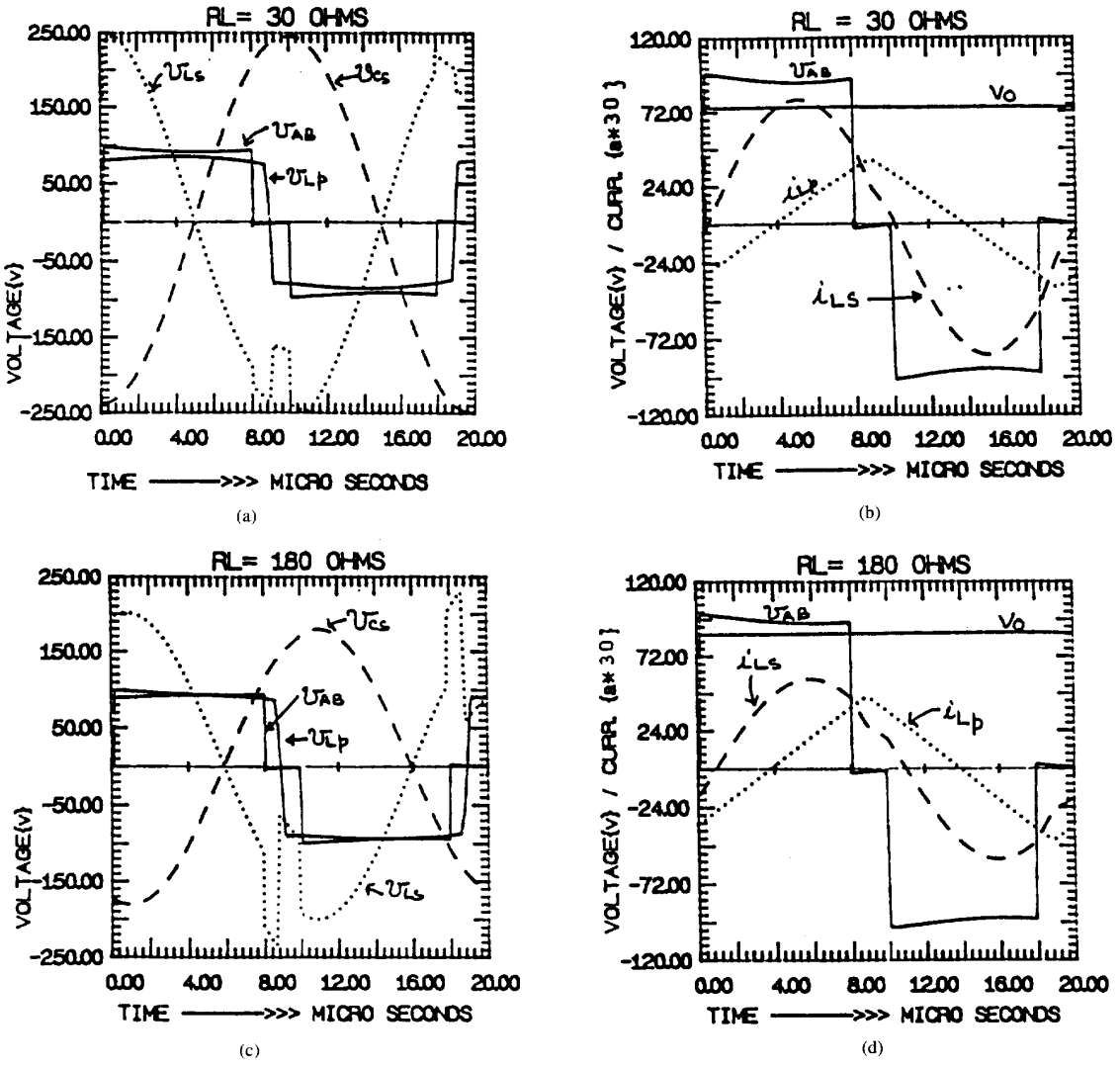

Fig. 10. Simulation waveforms for duty ratio of 0.8. (a) $R_L = 30\ \Omega v_{AB}, v_{Ls}, v_{cs}, v_{Lp}$. (b) $R_L = 30\ \Omega\ v_{AB}, i_{Ls}, i_{Lp}, V_o$. (c) $R_L = 180\ \Omega\ v_{AB}, v_{Ls}, v_{cs}, v_{Lp}$. (d) $R_L = 180\ \Omega\ v_{AB}, i_{Ls}, i_{Lp}, V_o$.

follows a sine function. These results are completely validated experimentally by plotting the variation of M_o with duty ratio as is shown in Fig. 6. At the optimum normalized switching frequency f_{no}, M_o is independent of variations in the load resistance for all pulse widths. However, in a practical setup there is a slight deviation in the experimental values when compared to the theoretical values as seen from Fig. 6 in the open-loop response of the voltage gain versus duty ratio of the LCL converter. This deviation increases with reducing values of load resistance or increasing values of load current for a given voltage. This arises because of sensing resistance of 0.5 Ω used in series with the resonant element for monitoring i_{Ls} and also finite resistance offered by diodes and MOSFET's in conduction. In order to maintain the output voltage constant at a desired value against the variations in the load resistance and supply voltage variations, the pulse width has to be changed in a closed-loop manner. However, the required change in pulse width to maintain constant output voltage against load variations and constant input voltage is very small.

The equivalent circuit of Fig. 3 along with the reflected load resistance $(8R_L/\pi^2)$ at the primary terminals of the transformer can be analyzed considering only the fundamental component of voltage and current. The expression for the voltage gain can be obtained and studied for load independent operation. It can be easily shown that the exercise leads to the optimum normalized switching frequency given by

$$f_{no} = \sqrt{1 + K_L}. \tag{16}$$

The frequency response of the equivalent circuit of the resonant converter for $K_L = 1$ and for different values of quality

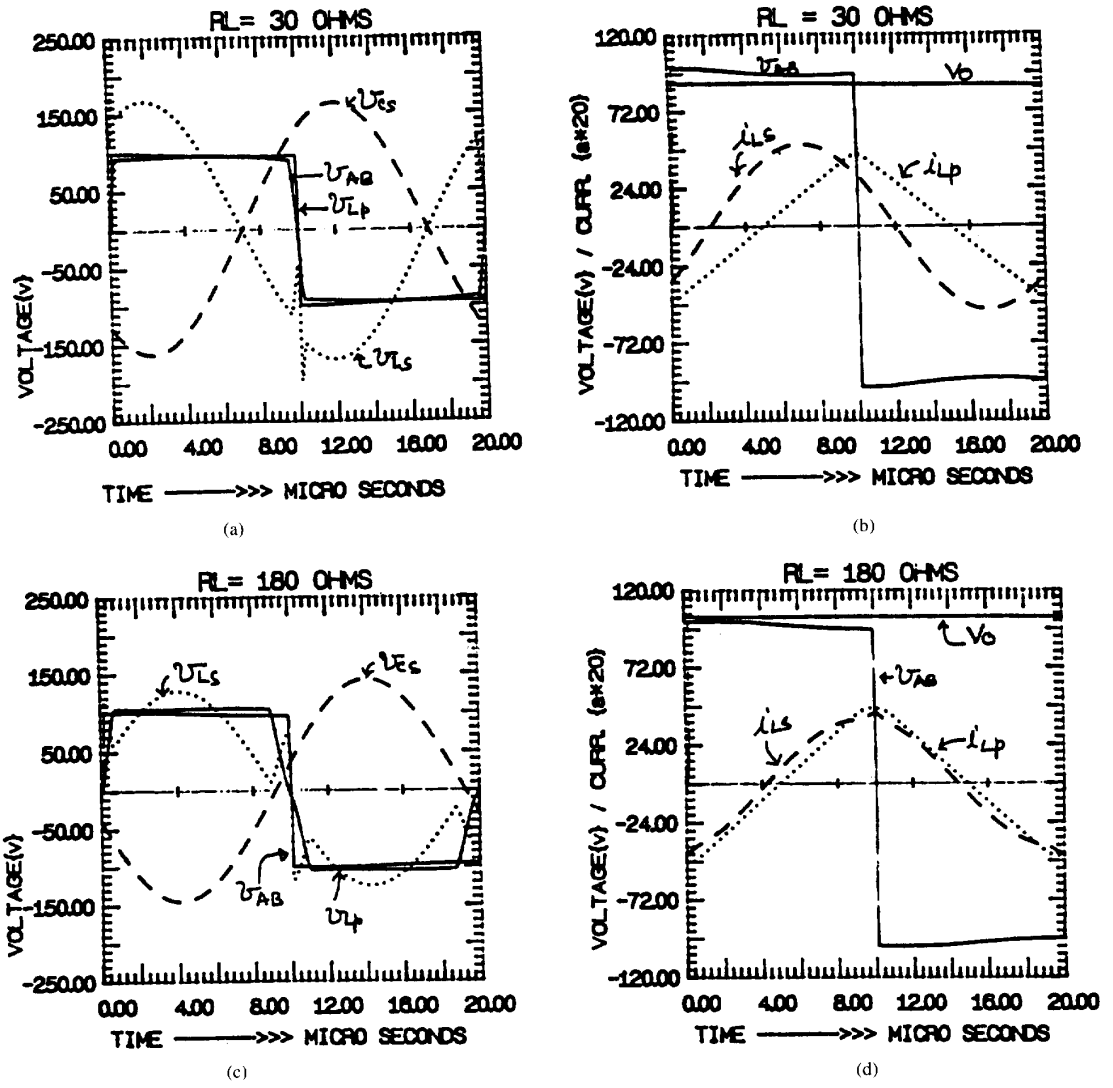

Fig. 11. Simulation waveforms for duty ratio of 1.0. (a) $R_L = 30\ \Omega$ $v_{AB}, v_{Ls}, v_{cs}, v_{Lp}$. (b) $R_L = 30\ \Omega$ $v_{AB}, i_{Ls}, i_{Lp}, V_o$. (c) $R_L = 180\ \Omega$ $v_{AB}, v_{Ls}, v_{cs}, v_{Lp}$. (d) $R_L = 180\ \Omega$ $v_{AB}, i_{Ls}, i_{Lp}, V_o$.

factor are shown in Fig. 7. The voltage gain is unity at the point of load independent operation. The normalized frequency corresponding to this operating point is dependent on the value of K_L.

IV. Simulation

The total converter is simulated using SPICE software package. MOSFET model 1 is used for simulating the active switch by changing the transconductance parameter (K_p) and mobility (U_o) of the standard model. The simulation is carried out for 120 μS which is equivalent to 6 cycles. The values obtained at the end of 6th cycle are fed back as initial values and the simulation is repeated again for the same number of cycles. This is continued several times until the steady state conditions are obtained for a given pulse width. Finally, the data is taken for the last cycle in the simulation interval. Figs. 8–11 show the steady state simulation waveforms for duty ratios 0.4 to 1.0 with an increment of 0.2, respectively. These waveforms are in agreement with the theoretical waveforms of Fig. 5 with negligible discontinuous conduction interval.

V. Design and Implementation

A. Choice of $K_L(L_p/L_s)$

If K_L is very small, the KVA rating of the resonant network increases for a given KW output due to large circulating current under light load conditions. On the other hand if K_L is large the KVA rating of the resonant network decreases at light loads. Under heavy load conditions the choice of large K_L is restricted for maintaining a lagging power factor.

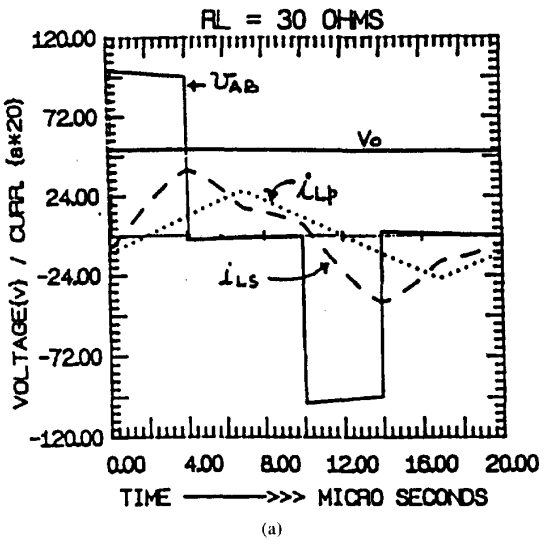

(a)

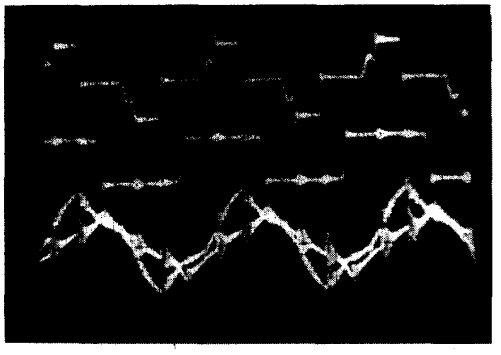

(b)

Fig. 12. Simulation and experimental waveforms for duty $D = 0.4$, $R_L = 30\ \Omega$. (a) Simulation. (b) Experimental: Top to bottom: v_{AB}, v_{Lp}, i_{Ls}, i_{Lp}. X-axis: 5 μs/div. Y-axis: v_{AB}, v_{Lp} ··· 100 V/div. i_{Ls}, i_{Lp} ··· 2 A/div.

Practically the converter is required to operate with a lagging power factor. That is, i_{Ls} should not become zero before $t = t_5$ (Fig. 2) when the duty is changed from 0 to 1 for all load conditions. However, at low duty ratio the free resonant interval $(t_5 - t_2)$ increases. Therefore, the mode 5 interval $(t_5 - t_4)$ also increases. In mode 5, the expression for the resonant current i_{Ls} is given by (2). As K_L increases, the initial current $i_{Ls}(t_4) = I_{LPM}$, decreases. Since it is the resonant network which supplies energy to the output load during this mode, there is a possibility that i_{Ls} may become zero before $t = t_5$ under heavy loading conditions. Thus the lagging PF operation can not be maintained. This can be verified from spice simulation waveforms and the experimental oscillograms for the same condition of $D = 0.4$, $R_L = 30\ \Omega$ as shown in Fig. 12. It can clearly be seen that i_{Ls} is marginally above zero level. Furthermore, when K_L is very large, the performance of the converter tends toward that of SRC which is not desirable. From the above considerations the value of K_L is taken as 1 in the

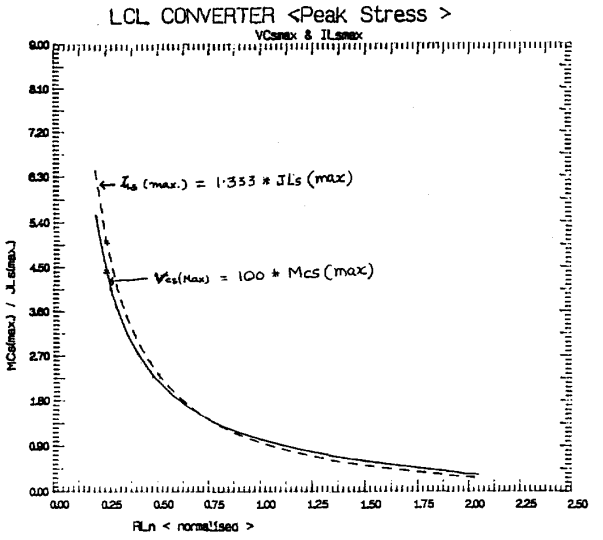

Fig. 13. Peak stresses of resonant components, V_{Cs}(max) and I_{Ls}(max).

experimental converter. It is desired to design the converter with the following specifications.

Power output: 133 Watts
Minimum input voltage: 100 V
Maximum output voltage: 100 V
Maximum load current: 1.33 A
Maximum overload current: 4 A
Inductance ratio (K_L): 1.0
Switching frequency (f_s): 50 kHz

The hf transformer turns ratio is assumed to be unity.

The load resistance, R_L = Maximum output voltage/Maximum output current

$$= \frac{100}{1.33} = 75\ \Omega. \tag{17}$$

The input rms voltage to the diode bridge = $V_{Lp} = 2\sqrt{2}V_o/\pi$.

The input rms current at the input of the diode bridge = $(\pi/2\sqrt{2})I_o$.

The reflected ac resistance on the input side of the diode bridge is

$$\frac{V_{Lp}}{I_d} = \frac{8V_o}{\pi^2 I_o} = \frac{8R_L}{\pi^2}. \tag{18}$$

For maximum power output

$$\sqrt{\frac{L_s}{C_s}} = \frac{8R_L}{\pi^2} = \frac{8 * 100}{\pi^2 1.333} = 60.8\ \Omega. \tag{19}$$

Since the switching frequency is 50 kHz

$$\frac{1}{2\pi\sqrt{L_s C_s}} = 50 * 10^3. \tag{20}$$

From (19) and (20)

$$C_s = 0.052\ \mu F, \quad L_s = 185\ \mu H. \tag{21}$$

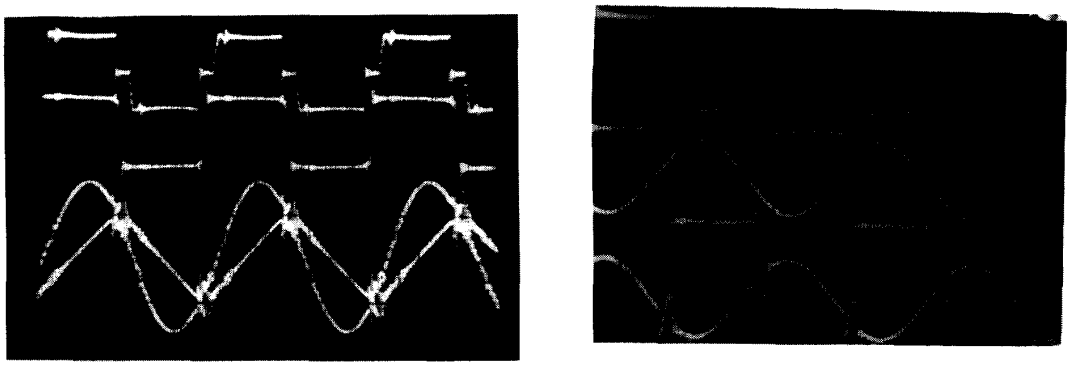

(a) (b)

Fig. 14. Experimental oscillograms for duty = 0.8. (a) $R_L = 30\ \Omega$: Top-bottom $v_{AB}, v_{Lp}, i_{Ls}, i_{Lp}$. (b) $R_L = 180\ \Omega$: Top-bottom $v_{AB}, v_{Lp}, v_{Cs}, v_{Ls}$. X-axis: 5 μ S/div. Y-axis: $v_{AB}, v_{Lp} \cdots$ 100 V/div.; $v_{Cs}, v_{Ls} \cdots$ 200 V/div.; $i_{Ls}, i_{Lp} \cdots 2$ A/div.

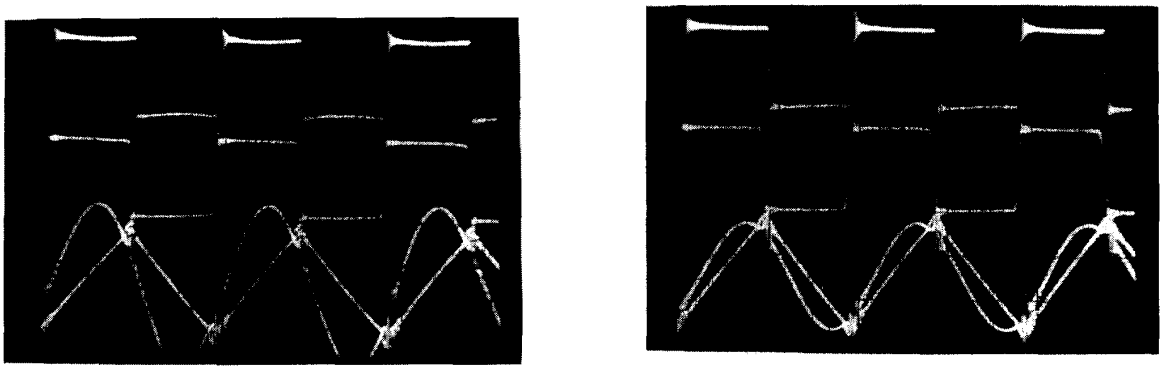

(a) (b)

Fig. 15. Experimental oscillograms for duty = 1.0. (a) $R_L = 30\ \Omega$: Top-bottom $v_{AB}, v_{Lp}, i_{Ls}, i_{Lp}$. (b) $R_L = 180\ \Omega$: Top-bottom $v_{AB}, v_{Lp}, i_{Ls}, i_{Lp}$. X-axis: 5 μ S/div. Y-axis: $v_{AB}, v_{Lp} \cdots$ 100 V/div.; $v_{AB}, v_{Lp} \cdots$ 100 V/div.; $i_{Ls}, i_{Lp} \cdots$ 2 A/div.

From the availability of the capacitors, C_s is chosen as 0.05 μF. Consequently from (20), the inductance L_s is obtained as 202 μH. In the experimental setup, the actual inductance used is 200 μH which is close to the designed value.

The peak voltages and currents are calculated using (2)–(6) for different load resistances. The base values for normalization are

Resistance: 75 Ω
Current: 1.33 A
Voltage: 100 V

Fig. 13 shows the variation of peak voltage and current with the load resistance. All quantities are represented in terms of normalized values.

The worst situation arises when the load current is maximum. Under this condition

$$R_L = 100/4 = 25\ \Omega. \tag{22}$$

The normalized load resistance is 0.333. From Fig. 13, the peak normalized values are

$$M_{Cs}(max) = 3 \cdot 24$$

$$J_{Ls}(max) = 3 \cdot 6.$$

In terms of actual values

$$i_{Ls}(max) = 3.6 * 1.333 = 4.8\ A$$

$$v_{Cs}(max) = 3.24 * 100 = 324\ V$$

Polypropylene capacitor of 0.05 μF/600 V is used for resonant capacitor C_s. FET IRF 330 is selected as the switching device which meets the peak current and voltage requirements.

Figs. 14–16 show experimental oscillograms from the setup for duty ratios 0.4, 0.8, and 1.0, respectively. The waveforms are obtained for two extreme values of load resistance of 30 Ω and 180 Ω. It has been observed experimentally that the waveforms are in good agreement with the simulation waveforms shown in Figs. 8–11 under similar operating conditions of load resistance and duty ratio. A careful observation of

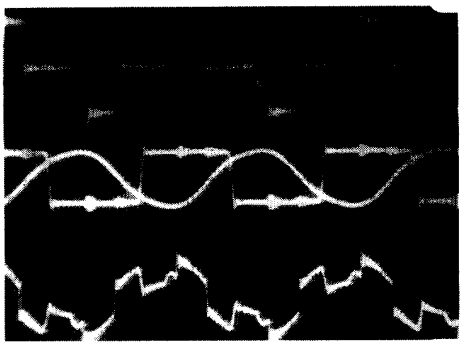

(a)

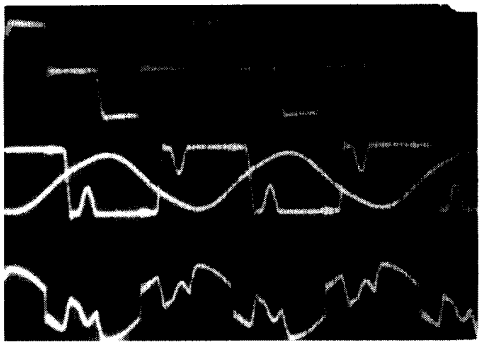

(b)

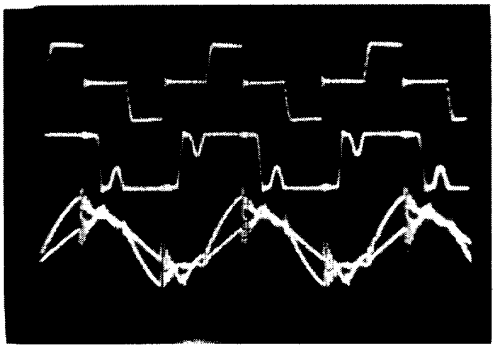

(c)

Fig. 16. Experimental oscillograms for duty = 0.4. (a) R_L = 30 Ω: Top-bottom $v_{AB}, ev_{Lp}, v_{Cs}, v_{Ls}$. (b) R_L = 180 Ω: Top-bottom $v_{AB}, v_{Lp}, v_{Cs}, v_{Ls}$. (c) R_L = 180 Ω: Top-bottom $v_{AB}, v_{Lp}, i_{Ls}, i_{Lp}$. X-axis: 5 $\mu S/div$. Y-axis: $v_{AB}, v_{Lp} \cdots$ 100 V/div.; $v_{Cs}, v_{Ls} \cdots /$ 200 V div.; $i_{Ls}, i_{Lp} \cdots$2 A/div.

simulation and experimental waveforms reveals the different modes of operation discussed in Section II. Fig. 17 shows the efficiency of the converter with respect to duty ratio. The efficiency reaches 96% at full duty ratio.

VI. Conclusion

The study of a three element LCL resonant converter with a voltage type load shows that it provides load independent operation above the resonant frequency theoretically. The results obtained from the experimental setup show that they are

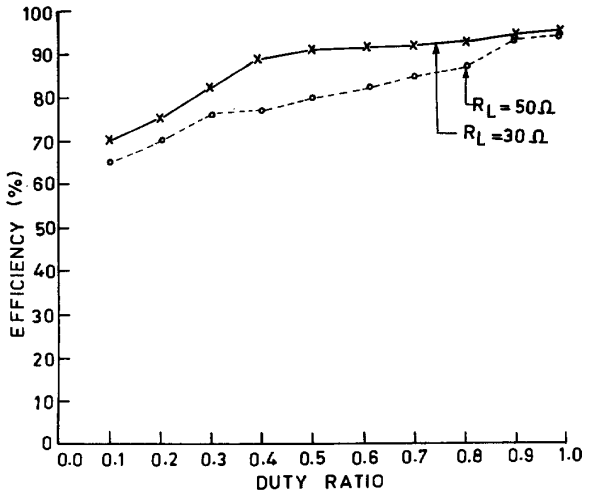

Fig. 17. Experimental results of efficiency variation with duty ratio of LCL converter.

close to the theoretical values taking practical considerations into account. Pulse width modulation is employed for the control and regulation of the output voltage. Contrary to conventional resonant converters, the switching frequency is held constant. Therefore, this allows the optimum choice of switching frequency from the standpoint of load independent operation. The good features of resonant circuit and pulsewidth modulation control have been exploited in this converter. Also, since the load independent point is above the resonant frequency where the operation is of lagging power factor, the switching power losses are minimized. With the addition of one more resonant element in the commonly used series resonant converter, the LCL resonant converter is potentially suited for applications such as space and radar high voltage power supplies with appropriate turns ratio of hf transformer. Another good feature of this converter is that the converter operation is not affected by the non idealities of the output transformer (magnetizing inductance) because of the additional resonant inductor L_p.

References

[1] J. G. Hayes, N. Mohan, and C. P. Henze, "Zero-voltage switching in a constant frequency digitally controlled dc-dc converter," *IEEE APEC*, 1988, pp. 360–366.

[2] T. H. Solane, "Design of high-efficiency series resonant converters above resonance," *IEEE Trans. Aerosp. Electron. Syst.*, vol. 26, pp. 393–402, Mar. 1990.

[3] A. K. S. Bhat, "A unified approach for the steady state analysis of resonant converters," *IEEE Trans. Power Electron.*, vol. PE-7, pp. 89–97, Jan. 1992.

[4] R. P. Severns, "Topologies for three element resonant converters," *IEEE Trans. Power Electron.*, vol. PE-7, pp. 89–97, Jan. 1992.

[5] F. G. Turnbull and R. E. Tompkins, "Design of a pulsewidth modulated resonant converter for high output voltage power supply," *IEEE Ind. Applicat. Soc. Annu. Meet.*, 1985, pp. 1145–1150.

[6] E. G. Schmidtner, "A new high switching frequency resonant converter topology," *High Frequency Power Conversion Conf. Rec.*, 1988, pp. 390–403.

[7] A. K. S. Bhat, "Analysis and design of LCL-type series resonant converter," *IEEE INTELEC*, 1990, pp. 172–178.

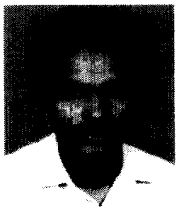

G. S. N. Raju received the B.Tech. degree in electronics engineering from Jawaharlal Nehru Technological University in 1976 and the M.Tech. degree from Indian Institute of Technology, Kanpur, in 1993.

Since 1977, he has been with Electronics and Radar Development Establishment (LRDE), Bangalore, involved in the design and devlopment of high voltage power supplies using resonant converters and high voltage high current pulse modulators used in radar transmitters. He was also responsible for the design and development of high power coherent transmitters using Klystrons, TWTS, and CFAS as final power amplifiers.

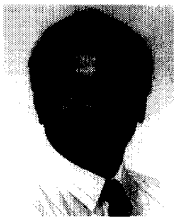

Seshagirirao Doradla (SM'87) received the B.E. (Honors) degree from Government College of Engineering, Kakinada, Andhra University, Waltair, India, in 1963, the M.E. degree from Jadavpur University, Calcutta, India, in 1967, and the Ph.D. degree from Queens University, Kingston, Ontario, Canada, in 1975. He was a Commonwealth Scholar during the Ph.D. Program.

He was a lecturer from 1967 to 1971 in the Department of Electrical and Electronics Engineering, Birla Institute of Technology and Science, Pilani, Rajasthan, India. He joined the Department of Electrical Engineering, Indian Institute of Technology, Kanpur, India, in 1976, where he is now a professor. He was with the Department of Electrical and Computer Engineering, Concordia University, Montreal, Canada as a Visiting Associate Professor from 1986–1988. He is presently with the Department of Electrical and Computer Engineering, University of Wisconsin-Madison as a Visiting Professor, taking one semester leave of absence from IIT Kanpur.

He is a co-author of *Thyristorised Power Controllers* published by Wiley Eastern Limited, New Delhi, India. His areas of interest include static power converters including resonant link inverters, power semiconductor drives, HVDC, FACTS, and static VAR compensators.